AGU PUBLICATIONS

Tectonics

RESEARCH ARTICLE
10.1002/2015TC003943

Key Points:
- The Eastern Karakoram has young apatite fission track dates and exhumes rapidly
- Exhumation rates increase from the Indus suture into the Karakoram
- Tectonic uplift increases surface elevation, glaciation, and rapid exhumation

Correspondence to:
D. Wallis,
eedw@leeds.ac.uk

Citation:
Wallis, D., A. Carter, R. J. Phillips, A. J. Parsons, and M. P. Searle (2016), Spatial variation in exhumation rates across Ladakh and the Karakoram: New apatite fission track data from the Eastern Karakoram, NW India, *Tectonics*, *35*, doi:10.1002/2015TC003943.

Received 8 JUN 2015
Accepted 23 FEB 2016
Accepted article online 27 FEB 2016

Spatial variation in exhumation rates across Ladakh and the Karakoram: New apatite fission track data from the Eastern Karakoram, NW India

David Wallis[1], Andrew Carter[2], Richard J. Phillips[1], Andrew J. Parsons[1], and Michael P. Searle[3]

[1]School of Earth and Environment, University of Leeds, Leeds, UK, [2]Department of Earth and Planetary Sciences, Birkbeck, University of London, London, UK, [3]Department of Earth Sciences, University of Oxford, Oxford, UK

Abstract Characterization of low-temperature cooling histories and associated exhumation rates is critical for deciphering the recent evolution of orogenic regions. However, these may vary significantly over relatively short distances within orogens. It is pertinent therefore to constrain cooling histories and hence exhumation rates across major tectonic boundaries. We report the first apatite fission track ages from the Karakoram Fault Zone in the Eastern Karakoram range, which forms part of the western margin of the Tibetan Plateau. Ten samples, from elevations of 3477–4875 m, have apatite fission track dates from 3.3 ± 0.3 Ma to 7.4 ± 1.1 Ma. The ages correspond to modeled average erosional exhumation rates of 0.67 + 0.27/−0.18 mm/yr across the Eastern Karakoram. The results are consistent with a trend northward from the Indus suture zone, across the Ladakh terrane and into the Karakoram, in which tectonic uplift associated with crustal thickening increases toward the north, raising elevation and promoting glaciation and generation of extreme relief. As a result, erosion and exhumation rates increase south to north. Present-day precipitation on the other hand varies little within the study area and on a larger scale decreases southwest to northeast across this portion of the orogen. The Eastern Karakoram results highlight the diverse patterns of exhumation driven by regional variations in tectonic response to collision along the western margin of Tibet.

1. Introduction

The Himalaya has been studied extensively to understand the links between tectonic and surface processes during mountain range evolution [e.g., *Godard et al*., 2014; *Lavé and Avouac*, 2001; *Molnar et al*., 1993; *Thiede and Ehlers*, 2013; *Wang et al*., 2014], and it has been suggested that coupling between high precipitation and tectonic strain may be necessary to facilitate exhumation of high-grade metamorphic units along the Greater Himalaya (Figure 1) [e.g., *Beaumont et al*., 2001; *Thiede et al*., 2004; *Zeitler et al*., 2001]. However, not all parts of the orogen appear to behave in this way. The Karakoram, bordering the western margin of the Tibetan Plateau, has extreme relief, variable topography (numerous peaks exceeding 7000–8000 m elevation, Figure 1), and has undergone exhumation of high-grade metamorphic rocks but is located in a relatively arid (present-day) climate (Figure 2). Unlike the adjacent Tibetan Plateau (Figure 1), which has low-relief and low-grade Paleozoic-Mesozoic sediments exposed at the surface [*Sinha et al*., 1999], the Karakoram is the most highly deformed and highest metamorphic grade portion of the former South Asian margin. This is reflected by young metamorphic, magmatic, and cooling ages [*Fraser et al*., 2001; *Searle et al*., 2010]. This portion of the orogen also has the thickest crust, reaching 75–80 km depth beneath the Karakoram Fault Zone (KFZ) [*Hazarika et al*., 2014; *Rai et al*., 2006] and 90 km depth beneath NW Tibet [*Wittlinger et al*., 2004]. However, the relationships between tectonic and surface processes in and around the Karakoram remain less extensively explored than in the Himalaya [*Bishop et al*., 2010; *Brozović et al*., 1997; *Korinkova et al*., 2014].

The Eastern Karakoram terrane occupies a key location at the junction of the Tibetan Plateau, the central Karakoram terrane, and the Ladakh terrane (Figure 1). Yet its exhumation history and morphological evolution remain comparatively enigmatic. The exposed rock types consist of medium- to high-grade metamorphic units and granitoids closely comparable to those exposed in the central Karakoram [*Phillips et al*., 2013; *Wallis et al*., 2014b] which has undergone recent and rapid exhumation [*Cerveny et al*., 1989; *Foster et al*., 1994] sufficient to expose sillimanite orthogneiss metamorphosed under conditions of 689 ± 48°C and 570 ± 190 MPa at only 5.4 ± 0.1 Ma [*Fraser et al*., 2001; *Searle et al*., 2010]. Farther southwest, the Ladakh arc terrane has experienced only an intermediate amount of exhumation (approximately 7–14 km) and shows a trend of decreasing apatite fission track (AFT) dates from approximately 30 Ma in the SW to approximately 6 Ma in the NE near the Karakoram Fault and the adjacent Eastern Karakoram terrane [*Kirstein*, 2011].

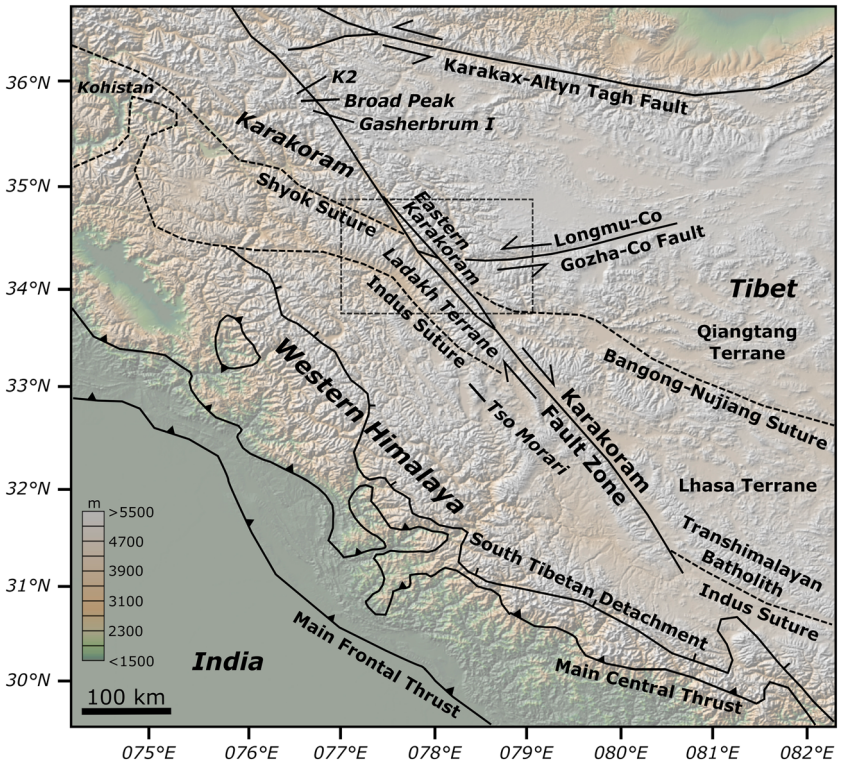

Figure 1. Simplified tectonic map of the Karakoram and western Himalaya and Tibet after *Searle et al.* [2011], overlaid on Global Multi-Resolution Topography data [*Ryan et al.*, 2009]. Dashed black box marks the location of Figure 3.

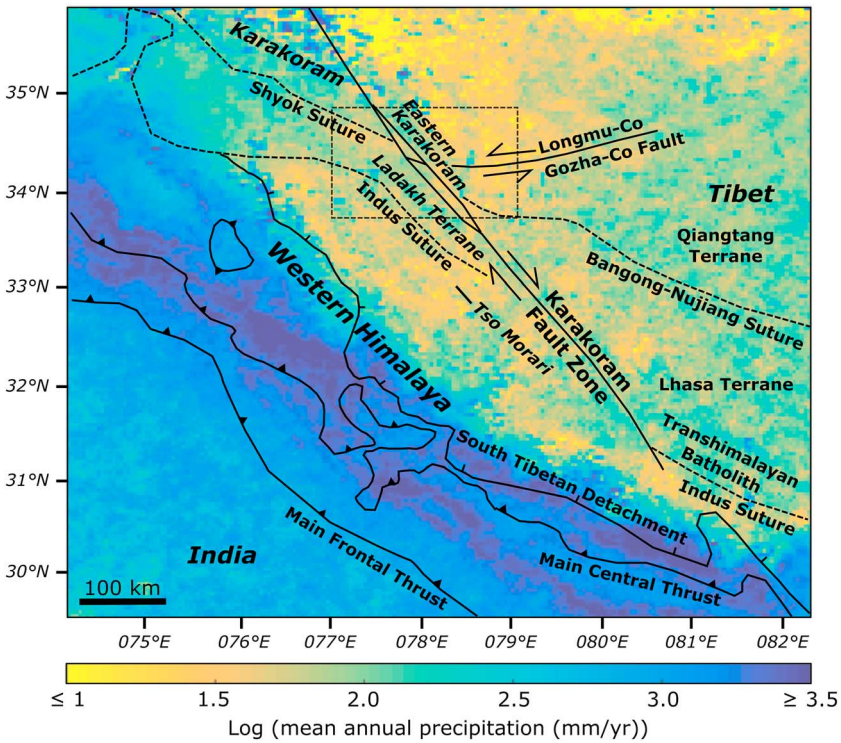

Figure 2. Mean annual precipitation data (1998–2009) from the Tropical Rainfall Measuring Mission [*Bookhagen and Burbank*, 2006] covering the same geographic area as Figure 1, with the exception of the northern edge for which there are no data. Dashed black box marks the location of Figure 3.

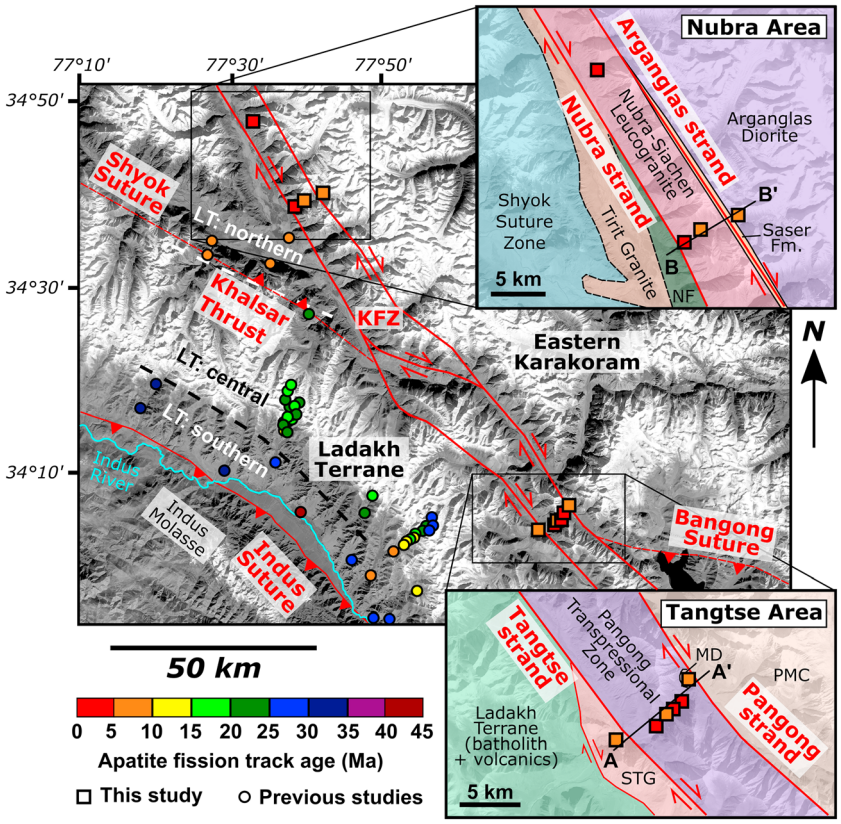

Figure 3. Simplified map of Ladakh, NW India, with Landsat 8, band 8 underlay showing December 2014 snow and ice cover (white). Apatite fission track sample locations from the present study (squares) and previous studies (circles) [*Clift et al.*, 2002; *Kirstein et al.*, 2006, 2009; *Kumar et al.*, 2007; *Sinclair and Jaffey*, 2001] are marked and color coded by fission track date. The sample groups of the southern, central, and northern Ladakh terrane (LT) of *Kirstein et al.* [2009] are indicated. A-A′ and B-B′ indicate the transects plotted in Figure 4. The Pangong Transpressional Zone includes (not differentiated) metamorphic country rocks of the Eastern Karakoram Metamorphic Complex, migmatites, and Cretaceous and Oligo-Miocene granitoids of the Karakoram batholith. KFZ = Karakoram Fault Zone, NF = Nubra formation, PMC = Pangong Metamorphic Complex, MD = Muglib Dome, and STG = South Tangtse granite.

Despite these varied patterns of exhumation across Ladakh and the Karakoram, few studies have investigated the relative influence of underlying factors such as regional tectonics, climatic gradients, or more localized deformation associated with specific geological structures [*Dortch et al.*, 2011b; *Kirstein et al.*, 2009]. In particular, it is yet to be established whether variations in exhumation rate follow long-range trends that cross geological boundaries or whether significant discontinuities exist at major faults. As such, it remains unclear whether patterns of uplift, erosion, cooling, and exhumation are internal to individual tectonic blocks or are characterized by longer-wavelength gradients that may instead reflect wider tectonic processes or climatic variation.

Current understanding of the Karakoram terrane is hindered by the lack of low-temperature thermochronological data, especially from the Eastern Karakoram. As a result, it is unknown whether exhumation of the Eastern Karakoram terrane was as rapid and as recent as that of the central Karakoram or whether it was somewhat more protracted and similar to the Ladakh terrane. A further complication is the potential influence of the KFZ, which dissects the Eastern Karakoram terrane and separates it from the central Karakoram and Ladakh terranes. Transpression within the KFZ may have locally uplifted portions of the Eastern Karakoram terrane during the mid-Miocene, potentially accelerating their exhumation [*Boutonnet et al.*, 2012; *Dunlap et al.*, 1998; *Searle and Phillips*, 2007; *Searle et al.*, 1998; *Wallis et al.*, 2014b]. This interpretation is based on ductile deformation fabrics, medium-temperature thermochronology, and juxtaposition of high-grade metamorphic rocks with different histories, but the lack of low-temperature thermochronological data from different portions of the Eastern Karakoram terrane, representing different fault blocks, prevents a more detailed understanding.

To address the lack of data from the Eastern Karakoram terrane, this paper presents new AFT dates from the Nubra and Tangtse areas in two transects across different fault blocks of the KFZ (Figure 3). The data allow us to test (1) the extent to which the KFZ has influenced the low-temperature cooling history of surrounding rock units in different fault blocks; (2) whether the Eastern Karakoram terrane follows the low-temperature cooling trend defined by the Ladakh terrane [*Kirstein et al*., 2009], whether it has undergone exhumation as rapid as the central Karakoram, or whether a significant discontinuity occurs across the KFZ; and (3) the relative significance of climatic gradients, regional tectonics, and/or localized deformation in producing the pattern of exhumation defined by the Ladakh, Eastern Karakoram, and central Karakoram terranes.

2. Geological Setting

2.1. Geology and Low-Temperature Cooling History of Ladakh and the Karakoram

In the regions bordering western Tibet (Figure 1), existing low-temperature thermochronological data are available from the Ladakh batholith, NW India [*Choubey*, 1987; *Clift et al*., 2002; *Kirstein et al*., 2006, 2009; *Kumar et al*., 2007; *Schulp et al*., 2003; *Sinclair and Jaffey*, 2001; *Sorkhabi et al*., 1994], and from the K2 gneiss and Gasherbrum Diorite in the central Karakoram, NE Pakistan [*Cerveny et al*., 1989; *Foster et al*., 1994].

The majority of the presently exposed intrusive lithologies of the Ladakh terrane were emplaced in an arc setting at 7–15 km depth between approximately 47 and 70 Ma, with emplacement ending soon after the India-Asia collision at approximately 50.5 Ma [*Kirstein*, 2011; *Najman et al*., 2010; *St-Onge et al*., 2010]. Synthesis of results from multiple thermochronometers ($^{40}Ar/^{39}Ar$ hornblende and biotite, fission track of titanite, zircon and apatite, and zircon and apatite (U-Th)/He) suggests that different portions of the Ladakh batholith have experienced variable and rather complex cooling histories [*Kirstein*, 2011]. However, AFT data from a transect across the batholith between the Indus suture in the south and the Shyok suture (Figure 3) in the north show a northward decreasing trend in cooling ages from 35–30 Ma to approximately 6 Ma [*Kirstein et al*., 2009]. *Kirstein et al*. [2009] proposed that Oligocene-Miocene southward tilting of the batholith resulted in asymmetrical topography, with greater elevation and stronger erosion in the north, whereas the southern margin was mantled by back thrusting of the Indus Molasse (Figure 3).

To the north, the central Karakoram terrane in Pakistan consists of the Paleozoic-Mesozoic Karakoram Metamorphic Complex intruded by the Karakoram batholith (Figure 1) [*Fraser et al*., 2001; *Searle*, 1991; *Searle et al*., 2010]. These include the amphibolite grade K2 gneiss and the Cretaceous Gasherbrum Diorite (Figure 1) [*Cerveny et al*., 1989; *Foster et al*., 1994; *Searle et al*., 1990]. Zircons from samples collected at elevations of 4880 m to 7165 m on Gasherbrum IV have fission track cooling ages of 125.0–31.4 Ma, the younger ages resulting from resetting by hydrothermal fluids [*Cerveny et al*., 1989]. These results demonstrate that the Gasherbrum Diorite has never been buried to depths of $>$6 km and, along with the extreme relief, suggest rapid and recent incision and exhumation [*Cerveny et al*., 1989]. This is borne out by apatite from samples collected at elevations of 5300 m to 8611 m on K2, which have fission track cooling ages of 2.1 $\pm$ 0.6 Ma to 4.3 $\pm$ 1.4 Ma, with one result of 31.5 $\pm$ 5.6 Ma [*Foster et al*., 1994]. Again, these data suggest rapid apparent denudation (approximately 3–6 mm/yr) commencing after 5 Ma [*Foster et al*., 1994] and demonstrate that the central Karakoram has experienced a markedly different low-temperature cooling history from the Ladakh batholith to the south. *Searle and Phillips* [2007] noted that while the Cretaceous-Paleogene cooling/exhumation history of the K2-Broad Peak-Gasherbrum region of the central Karakoram was unrelated to activity on the adjacent KFZ, local transpressional motion on this structure may have contributed to rapid exhumation in the K2-Gasherbrum range since 4.3 $\pm$ 1.4 Ma.

The Eastern Karakoram range in northern India is separated from both the Ladakh terrane and the central Karakoram by the NW-SE striking dextral KFZ (Figure 1). Several studies have examined the medium-high temperature cooling history of the Eastern Karakoram terrane using hornblende, biotite, muscovite, and K-feldspar $^{40}Ar/^{39}Ar$ thermochronology [*Bhutani et al*., 2003; *Boutonnet et al*., 2012; *Dunlap et al*., 1998; *Mukherjee et al*., 2012; *Searle et al*., 1998] as well as geothermobarometry and U/Pb zircon dating [*Phillips et al*., 2013; *Wallis et al*., 2014b]. These studies indicate cooling of the Eastern Karakoram from ~700 to 300°C during the Miocene and are discussed in detail below. However, there are currently no low-temperature thermochronological data available to constrain the latter stages of cooling and exhumation of the Eastern Karakoram terrane.

2.2. Geology of the Eastern Karakoram

The Eastern Karakoram range delineates the western margin of the Tibetan Plateau in Ladakh, NW India, and is accessible in the regions around Tangtse village in the SE and the Nubra Valley in the NW (Figure 3). The Eastern Karakoram terrane consists of the Eastern Karakoram Metamorphic Complex, which underwent kyanite-grade metamorphism at up to 736 ± 47°C and 1059 ± 219 MPa, followed by multiple subsequent metamorphic events during exhumation, including 17.4 ± 0.4 Ma migmatization at 688 ± 44°C and 522 ± 91 MPa [*Phillips et al*., 2013; *Rutter et al*., 2007; *Streule et al*., 2009; *Wallis et al*., 2014b]. The Eastern Karakoram Metamorphic Complex is subdivided into the Nubra and Saser formations in the Nubra region and the Pangong Metamorphic Complex and Pangong Transpressional Zone (PTZ) in the Tangtse region (Figure 3). In NW India, these units form the county rock to the Karakoram batholith, composed of Cretaceous I-type granitoids produced during Tethyan subduction and Miocene S-type granitoids resulting from postcollisional crustal anatexis (Figure 3) [*Phillips et al*., 2013; *Reichardt et al*., 2010; *Searle et al*., 1998, 2010].

The KFZ is a >800 km long, NW-SE striking, dextral strike-slip fault system extending from the Pamir in the NW to the Mount Kailas region in the SE (Figure 1). In its central portion, the KFZ juxtaposes the Eastern Karakoram terrane against the Ladakh terrane and consists of the Nubra and Arganglas fault strands (Nubra region) which link with the Tangtse and Pangong strands (Tangtse region) respectively across a major left-stepping jog (Figure 3).

Estimates of the age, offset, and long-term slip rate of the KFZ vary widely and can be generalized into two end-member models [*Searle et al*., 2011]. In one, the KFZ has accommodated offset of up to 250–565 km at slip rates of >10 mm/yr since initiating as early as >22 Ma [*Boutonnet et al*., 2012; *Lacassin et al*., 2004; *Leloup et al*., 2011; *Sen et al*., 2014]. In the other, the fault has accommodated offsets of less than 150 km at slip rates of <10 mm/yr, initiating after 15.68 ± 0.5 Ma [*Phillips et al*., 2004; *Searle*, 1996; *Searle and Phillips*, 2007; *Searle et al*., 1998, 2011; *Wallis et al*., 2014a, 2014b; *Wang et al*., 2012, 2013; *Zhang et al*., 2011]. Estimates of both the Quaternary and present-day slip rates of the KFZ span 0–11 mm/yr [*Banerjee and Bürgmann*, 2002; *Brown et al*., 2002; *Chevalier et al*., 2012; *Jade et al*., 2004, 2010; *Robinson*, 2009; *Wang and Wright*, 2012]. Paleoseismic evidence suggests that large earthquakes have occurred on both the Nubra ($M_w > 6$) and Pangong (M_w 7–8) strands of the fault during the Quaternary [*Brown et al*., 2002; *Phartiyal and Sharma*, 2009; *Phartiyal et al*., 2005; *Upadhyay*, 2001, 2003].

Deformation fabrics unequivocally attributable to the KFZ, and preserved in exposed fault rocks, formed under conditions spanning approximately 550°C (approximately 15 km depth according to the Miocene geothermal gradient of *Wallis et al*. [2014b]) to a few kilometers depth [*Phillips and Searle*, 2007; *Wallis et al*., 2013]. Deformation microstructures in such fault rocks demonstrate KFZ kinematics consistently dominated by dextral strike slip since the mid-Miocene [*Searle et al*., 1998; *Phillips and Searle*, 2007; *Wallis et al*., 2013], while major restraining bends are associated with transpressional zones tens of kilometers in fault-parallel length, e.g., the PTZ in the Eastern Karakoram terrane (Figure 3) [*Searle and Phillips*, 2007; *Searle et al*., 1998].

In the Tangtse region, the Pangong Transpressional Zone is predominantly bounded by the Tangtse and Pangong strands of the KFZ, which juxtapose it with the Ladakh terrane to the SW and the Pangong Metamorphic Complex to the NE, respectively (Figure 3). The PTZ is an approximately 7 km wide zone of predominantly amphibolite facies metamorphic lithologies, including migmatites, intruded by Cretaceous I-type granitoids and Miocene leucogranitoids [*Phillips et al*., 2013; *Reichardt and Weinberg*, 2012; *Wallis et al*., 2014b]. Ductile deformation fabrics occur commonly across the PTZ and range from localized mylonitic shear zones to pervasive gneissosity. Although cataclastic fault rocks are rare within the PTZ, the Pangong strand at its NE margin contains an approximately 10 m wide zone of fault gouge [*Rutter et al*., 2007]. *Boutonnet et al*. [2012] interpreted deformation to have localized northeastward toward the Pangong strand (their "Muglib strand") as the region was exhumed.

In the Nubra area, the Nubra and Arganglas strands of the KFZ bound the 5–7 km wide, 15.55 ± 0.74 Ma Nubra-Siachen leucogranite (Figure 3) [*Phillips et al*., 2004]. The Nubra strand follows the SW margin of this leucogranite along its contact with the metavolcanosedimentary Nubra formation [*Phillips et al*., 2004]. Farther SW, the Nubra formation contacts the 68 ± 1 Ma Tirit granite and the Ladakh terrane [*Weinberg et al*., 2000]. The Arganglas fault strand follows the NE margin of the Nubra-Siachen leucogranite at its contact with the adjacent kilometer-thick Saser formation [*Phillips and Searle*, 2007; *Wallis et al*., 2013]. Farther NE, the Saser formation is intruded by the 108.6 ± 1.7 Ma Arganglas Diorite [*Phillips et al*., 2013]. Deformation in this

area is confined to the Nubra and Arganglas fault strands, while the Tirit granite, interior of the Nubra-Siachen leucogranite, and the Arganglas Diorite are relatively undeformed.

2.3. Geomorphological Overview

Both elevation and relief generally increase from the Ladakh terrane to the Eastern Karakoram terrane and increase further again in the central Karakoram terrane. The Ladakh terrane forms an orogen-parallel range between approximately 3300 m and 6000 m elevation (Figure 1). The adjacent Eastern Karakoram range consists of a NW-SE trending range (Figure 1) with maximum relief of approximately 4300 m between the highest summits (up to 7672 m elevation) and the valley bottoms (approximately 3300 m elevation). Farther north, the central Karakoram range has extreme relief of up to 4700 m from the summit of K2 (8611 m elevation) to adjacent valley bottoms (~3900 m elevation).

Present-day precipitation across the Ladakh and Karakoram ranges is low ($<$300 mm/yr) with relatively little spatial variation, but the larger-scale trend is one of precipitation decreasing from SW to NE from the frontal Himalaya ($>$1000 mm/yr) into the Asian interior ($<$100 mm/yr, Figure 2) [*Bookhagen and Burbank*, 2006, 2010; *Dortch et al*., 2013; *Palazzi et al*., 2013]. Drainage is typically dominated by snow and glacial meltwater, although rare local convective storm events occur [*Hobley et al*., 2012].

The highest elevations of the Ladakh Range host small cirque glaciers which are more numerous on the north side of the range and all of which originate on north facing slopes [*Dortch et al*., 2011b]. *Dortch et al*. [2011b] found that glacial equilibrium line altitudes closely mimic the distribution of highest elevation across the Ladakh Range, consistent with the "glacial buzzsaw hypothesis" in which efficient glacial erosion exerts a strong influence on topographic elevation [*Egholm et al*., 2009; *Thomson et al*., 2010]. The Eastern Karakoram range has more extensive glacial cover, with glaciers originating on slopes facing all directions and individual glaciers commonly reaching $>$10 km length. The central Karakoram range has the greatest glacial cover, hosting several of the world's longest glaciers outside the polar regions, including the $>$70 km long Siachen glacier which divides the central and Eastern Karakoram ranges.

3. Methodology

Samples were collected from two transects across the central KFZ in the Tangtse and Nubra areas (Figure 3). Additional samples from SW of the Nubra strand (i.e., similar to the location of sample Tiri 3240 of *Kirstein et al*. [2009]) were considered for AFT dating but did not contain suitable apatites. The Nubra transect forms a northeastern continuation of the Ladakh batholith transect (Figure 3) of *Kirstein et al*. [2006, 2009] and *Kirstein* [2011] and extends these previous results across the KFZ within the Eastern Karakoram terrane. Sample W11/12 was collected 20 km northwest from the other three samples of the main Nubra transect. The Tangtse transect contains the major Pangong Transpressional Zone of the KFZ [*Phillips*, 2008; *Searle et al*., 1998], allowing its low-temperature cooling history to be constrained and compared to that of the Nubra area where evidence for transpressional fault motion is more limited [*Wallis et al*., 2015].

One sample (W11/47) was collected from the NE of the KFZ in the Nubra transect. However, it was not possible to obtain samples from NE of the KFZ in the Tangtse transect due to a lack of suitable lithologies in the Pangong Metamorphic Complex to the NE of the Pangong fault strand. Due to limited access, it was not possible to obtain samples from the region farther NE of the KFZ.

Sample details are given in Table 1. Samples were collected from valley bottoms and low elevations on valley sides. Samples from the Tangtse transect are from a narrow range of elevations between 4000 m and 4189 m. Samples from the Nubra transect span a greater range of elevations, increasing from 3477 m in the Nubra valley to 4875 m in the Eastern Karakoram range. All samples consist of either Cretaceous or Miocene granitoids of the Karakoram batholith.

For this study we used AFT thermochronometry to constrain rates of rock cooling. The effective closure temperature (for steady cooling through the AFT partial retention zone) is around 110–130°C, the exact value depending on the cooling rate to the surface [e.g., *Reiners and Brandon* [2006]]. Apatite grains were extracted from the rock samples using conventional magnetic and heavy liquid separation techniques then mounted in epoxy resin on glass slides and polished for etching to reveal the natural spontaneous fission tracks. The apatites were etched using 5 N HNO_3 at 20°C for 20 s. Etched grain mounts were then packed with mica

Table 1. Sample Details[a]

Sample	Lithology	Unit	Distance From Nubra/Tangtse Strand (m, NE Positive)	Elevation (±25 m)	UTM Grid Reference
Tangtse transect					44 N
W11/113	Hbl + Bt granite	STG	-900	4189	0238345 3767930
W11/80	Bt leucogranite	PTZ	2100	4000	0241552 3768594
W11/63	Bt leucogranite	PTZ	3500	4037	0242490 3769683
W11/60	Diorite	PTZ	4050	4012	0242976 3769954
W11/74	Gr. leucosome	PTZ	5100	4072	0243761 3770691
W10/23	Bt leucogranite	PTZ	6600	4090	0244380 3772336
Nubra transect					43 N
W11/26	Bt leucogranite	NSL	15	3477	0742019 3835401
W11/12	Bt leucogranite	NSL	1050	3637	0733308 3853035
W11/41	Bt leucogranite	NSL	1900	4012	0743591 3836486
W11/47	Diorite	AD	6250	4875	0747605 3838179

[a]NSL = Nubra-Siachen leucogranite, AD = Arganglas Diorite, STG = south Tangtse granite, and PTZ = Pangong Transpressional Zone.

external detectors and corning glass (CN5) dosimeters and irradiated in the FRM 11 thermal neutron facility at the University of Munich in Germany. Following irradiation, the external detectors were etched using 48% HF at 20°C for 25 min. Sample ages were determined using the zeta calibration method and International Union of Geological Sciences-recommended age, standards [*Hurford*, 1990]. As the samples were characterized by low spontaneous track densities due to their young age, as many grains were counted as possible in order to suitably capture the natural Poisson distribution and obtain good counting statistics. Table 2 summarizes the AFT results.

Erosional exhumation rates were estimated from AFT ages using the nonsteady state, eroding half-space model of *Willett and Brandon* [2013]. This approach is suitable for regions where exhumation results from erosional denudation with negligible tectonic removal of overlying material (i.e., by normal faulting). This is a reasonable approximation for the central KFZ which, unlike the southern KFZ, lacks a significant extensional component and is dominated by strike-slip kinematics [e.g., *Wallis et al*. [2013]]. While Miocene transpressional motion resulted in enhanced uplift of the PTZ relative to the adjacent Ladakh terrane and Pangong Metamorphic Complex [*Phillips and Searle*, 2007; *Searle et al*., 1998; *Wallis et al*., 2014b], recent deformation in the region is dominated by strike-slip kinematics [*Brown et al*., 2002].

Erosion rates were calculated for the 10 Eastern Karakoram terrane samples and also, for comparison, the 12 AFT dates from the Ladakh batholith reported by *Kirstein et al*. [2009]. The Ladakh batholith data set was considered in three portions, the southern, central, and northern batholith, as defined by *Kirstein et al*. [2009]. The *Willett and Brandon* [2013] approach incorporates both the cooling rate dependence of closure temperature (i.e., partial annealing zone) and thermal advection by rock motion toward the Earth's surface. The model

Table 2. Apatite Fission Track Results[a]

			Dosimeter		Spontaneous		Induced		Age Dispersion		Central Age (Ma)
Sample Number	Elevation (±25 m)	N	ρ_d	N_d	ρ_s	N_s	ρ_i	N_i	$P\chi^2$	$RE_{\%}$	±1 s
					Tangtse Transect						
W11/113	4189	30	1.579	4378	0.046	154	2.430	8389	0.02	45.3	5.1 ± 0.6
W11/80	4000	34	1.579	4378	0.036	115	1.972	6688	1.9	36.8	4.7 ± 0.5
W11/63	4037	30	1.579	4378	0.094	228	4.473	11300	86.5	0.6	5.4 ± 0.4
W11/60	4012	40	1.579	4378	0.044	131	2.70	8589	14.2	20.4	4.1 ± 0.4
W11/74	4072	40	1.579	4378	0.032	119	1.663	6479	18.9	0.7	4.9 ± 0.5
W10/23	4090	30	1.579	4378	0.086	206	4.022	10278	84.7	0.4	5.3 ± 0.4
					Nubra Transect						
W11/26	3477	23	1.579	4378	0.070	91	3.556	5183	3.4	35.3	4.8 ± 0.6
W11/12	3637	30	1.579	4378	0.096	169	7.175	13548	28.7	14.5	3.3 ± 0.3
W11/41	4012	35	1.579	4378	0.096	281	4.549	13861	23.8	15.7	5.4 ± 0.4
W11/47	4875	23	1.579	4378	0.141	133	4.922	4773	63.1	1.1	7.4 ± 1.1

[a]N = number of grain analyzed, $\rho(d, s, i)$ = track density, N(d, s, i) = number of tracks, $P\chi^2$ = probability of obtaining χ^2 value for v degrees of freedom, where $v = N - 1$, and $RE_{\%}$ = age dispersion around central age.

Table 3. Modeled Erosional Exhumation Rates and Estimated Local Mean Elevations Used in the Erosion Rate Calculation[a]

Sample	Distance From Indus River (km)	Mean elevation in 10 km Radius (m)	Maximum Age, 40°C/km (mm/yr)	Central Age, 35°C/km (mm/yr)	Minimum Age, 30°C/km (mm/yr)
		Tangtse Transect, Eastern Karakoram			
W11/113	39	4640	0.49	0.67	0.95
W11/80	42	4646	0.50	0.68	0.97
W11/63	43.2	4689	0.44	0.58	0.79
W11/60	43.7	4755	0.56	0.77	1.09
W11/74	44.8	4759	0.47	0.64	0.91
W10/23	46.3	4783	0.44	0.58	0.80
Mean			0.48	0.65	0.92
		Nubra Transect, Eastern Karakoram			
W11/26	56.5	4123	0.48	0.67	0.97
W11/12	69.7	4328	0.74	1.01	1.43
W11/41	58.2	4477	0.48	0.62	0.84
W11/47	62.1	5110	0.35	0.48	0.69
Mean			0.51	0.70	0.98
		Northern Ladakh Batholith			
Disk 3220	44.7	3956	0.24	0.41	0.85
Dok 3525	41.7	4091	0.31	0.55	1.27
Hund 3250	45.1	3945	0.31	0.46	0.73
Tiri 3240	49.1	3791	0.29	0.45	0.78
Mean			0.29	0.47	0.91
		Central Ladakh Batholith			
Khar 3975	36.8	4375	0.10	0.14	0.22
Khar 4918	24.1	5066	0.13	0.18	0.24
Nang 3555	9.9	3951	0.10	0.14	0.18
Nang 4300	10.0	4708	0.11	0.15	0.19
Mean			0.11	0.15	0.21
		Southern Ladakh Batholith			
BAS1	7.5	4039	0.06	0.08	0.10
BAS 4001	12.2	4370	0.06	0.08	0.12
LEH 3295	1.1	3703	0.07	0.09	0.12
Karu 3400	2.7	3836	0.07	0.09	0.12
Mean			0.07	0.09	0.12

[a]Erosion rates modeled using age2edot [*Willett and Brandon*, 2013]. Data for Ladakh batholith samples are taken from *Kirstein et al.* [2009]. Exhumation rates estimated for central apatite fission track ages and upper and lower age error bounds, combined with geothermal gradients of 35°C/km, 40°C/km, and 30°C/km, respectively, to gauge uncertainty.

inputs are the duration of erosion, mean surface temperature, deviation of sample elevation from mean elevation, thermochronometric age, and geothermal gradient. The duration of erosion was set to 20 Myr for the Eastern Karakoram samples and 50 Myr for Ladakh batholith samples, broadly consistent with existing geological and thermochronological constraints [*Boutonnet et al.*, 2012; *Kirstein*, 2011]. Mean surface temperature was set to 0°C based on the mean temperature in Ladakh during the twentieth century [*Bhutiyani et al.*, 2007]. The mean elevation in the vicinity of each sample (Table 3) was calculated from Advanced Spaceborne Thermal Emission and Reflection Radiometer Global Digital Elevation Model (ASTER GDEM) data for a circular area of 10 km radius centered on each sample, following *Willett and Brandon* [2013]. *Wallis et al.* [2014b] estimated the geothermal gradient in the Eastern Karakoram to have been 36 ± 7°C/km during the Miocene; therefore, estimates of erosion rate were calculated for geothermal gradients of 30, 35, and 40°C/km. The erosion rate estimates reported herein are based on the 35°C/km geothermal gradient and central fission track age. Upper bound erosion rate uncertainties were derived from a 30°C/km geothermal gradient and lower bound ages. Lower bound erosion rate uncertainties were derived from a 40°C/km geothermal gradient and upper bound ages.

4. Results

AFT dates for the Tangtse area samples (Table 2) range from 4.1 ± 0.4 Ma (W11/60) to 5.3 ± 0.4 Ma (W10/23). Several samples have greater than 20% dispersion in grain ages about the central age due to the low (0 or 1)

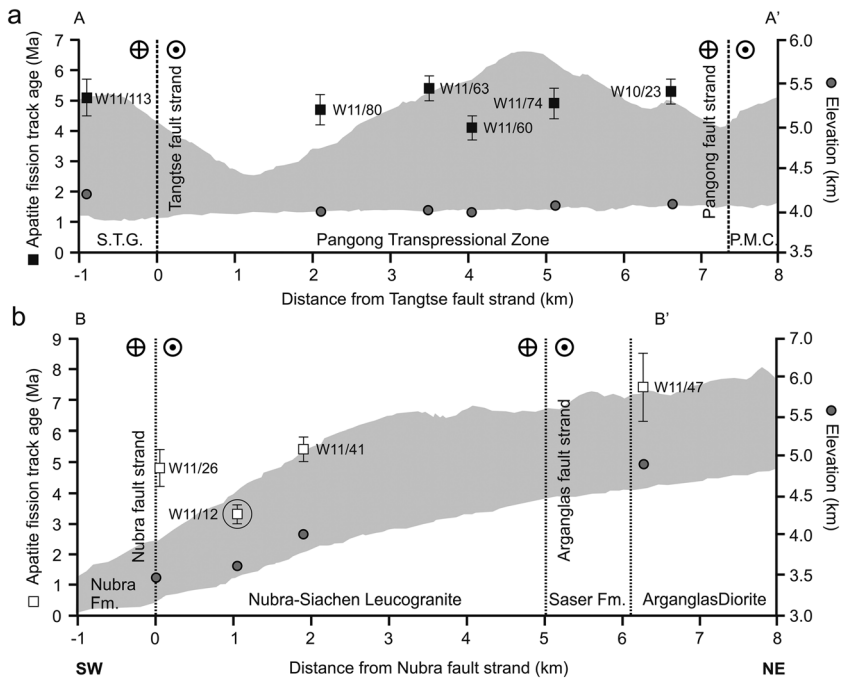

Figure 4. Apatite fission track ages in the (a) Tangtse (A-A′) and (b) Nubra (B-B′) transects across the Karakoram Fault Zone. Sample apatite fission track ages and elevations are projected onto linear transects (A-A′ and B-B′) marked in Figure 3. Sample W11/12, which lies off the main B-B′ transect, is circled. Grey region marks the range of elevation in a 6 km wide swath along the transects from ASTER GDEM data. ASTER GDEM is a product of The Ministry of Economy, Trade, and Industry of Japan and NASA. Also shown are the positions of major fault strands and simplified lithological unit divisions.

spontaneous track counts in some grains. Examination of grain age distributions (radial plots) confirms that there are no spurious grain ages nor distinct populations that might alternatively explain the overdispersion. The dates show no systematic trend along the transect, and sample W11/113 from SW of the Tangtse fault strand shows no significant difference from the samples within the PTZ to the NE of the Tangtse strand (Figure 4). The Tangtse area samples do not show a systematic age-elevation relationship (Figure 5), due to their limited range of sample elevations (4000–4189 m).

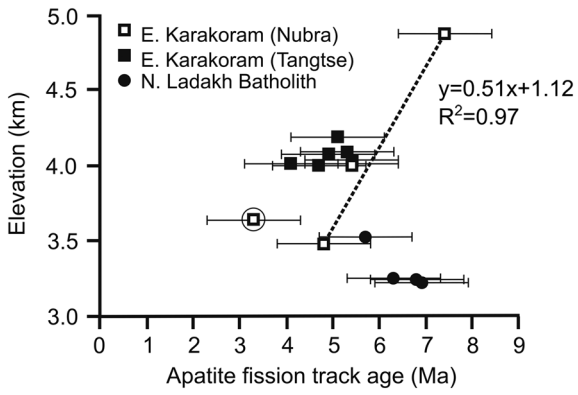

Figure 5. Age-elevation relationship for the Eastern Karakoram samples. Dashed line shows linear best fit through the data from the three Nubra samples that line on the main B-B′ transect. Sample W11/12, which lies off the main B-B′ transect, is circled. Data for the northern Ladakh batholith from *Kirstein et al.* [2009] are included for comparison with the Nubra results.

Dates for the Nubra area samples (Table 2) range from 3.3 ± 0.3 Ma (W11/12) to 7.4 ± 1.1 Ma (W11/47), generally increasing along transect, from the Nubra valley in the SW to the Arganglas Diorite in the NE (Figure 4). The three samples which lie on the main B-B′ transect, obtained from elevations between 3477 m and 4875 m, show a positive age-elevation relationship (Figure 5). Sample W11/12, collected 20 km NW from the main transect, shows a younger age for its elevation than the other samples.

Erosion rates estimated for the Tangtse area samples range between 0.58 + 0.21/−0.14 mm/yr (W11/63) and 0.77 + 0.32/−0.21 mm/yr (W11/60) and average 0.65 + 0.27/−0.17 mm/yr (Table 3 and Figure 6). Erosion rates estimated for the Nubra area samples range between 0.48 + 0.21/−0.13 mm/yr (W11/47) and 1.01 + 0.42/−0.27 mm/yr (W11/12) and average 0.70 + 0.29/−0.18 mm/yr (Table 3). The average

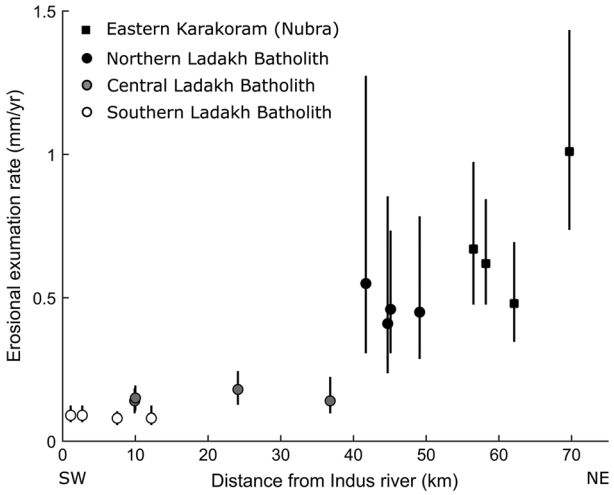

Figure 6. Variation in modeled erosional exhumation rates across the Ladakh batholith and Eastern Karakoram with distance from the Indus River. Exhumation rates were estimated using the eroding half-space model of *Willett and Brandon* [2013] for apatite fission track data from the Ladakh batholith ($n = 12$, AFT data from *Kirstein et al*. [2009]) and Nubra area of the Eastern Karakoram ($n = 4$, this study).

erosion rate estimate for the northern Ladakh batholith is $0.47 + 0.44/-0.18$ mm/yr (Table 3). That of the central portion of the batholith is $0.15 + 0.06/-0.04$ mm/yr, while that of the southern margin is $0.09 + 0.03/-0.02$ mm/yr (Table 3 and Figure 6). The uncertainties in exhumation rate, apparent in Figure 6, are larger for younger samples because the uncertainties in both age and geothermal gradient have a proportionally greater impact for samples with younger central ages.

5. Discussion

5.1. Cooling and Exhumation of the Eastern Karakoram Terrane Within and Across the Karakoram Fault Zone

The Tangtse transect crosses the Tangtse strand of the KFZ, while the Nubra transect crosses the Arganglas strand and also provides a continuation of the results of *Kirstein et al*. [2009] across the Nubra strand. This allows us to look for differences in cooling histories across these strands. The lack of significant age differences between sample W11/113 and those across the Tangtse strand (Figure 4) suggests that no significant differential exhumation has occurred across this fault strand or the PTZ since approximately 4–5 Ma. This is consistent with the limited structural evidence for low-temperature deformation on the Tangtse strand and within the PTZ [*Rutter et al*., 2007; *Wallis et al*., 2013].

The AFT date of the Arganglas Diorite (7.4 ± 1.1 Ma), NE of the Arganglas strand, differs from samples of the Nubra-Siachen leucogranite to the SW of the fault strand ($<5.4 \pm 0.4$ Ma, W11/41; Figure 4). However, samples in this transect span an elevation range of 1398 m and show a positive age-elevation relationship (Figure 5). Also, the Arganglas strand displays only minor low-temperature deformation structures, such as centimeter-thick cataclasite-filled faults [*Wallis et al*., 2013]. Therefore, we interpret the age variation within the Nubra transect and across the Arganglas strand to result from erosional exhumation of samples at different structural levels (i.e., paleodepths), rather than differential exhumation across the Arganglas strand.

The Nubra transect samples from the Eastern Karakoram terrane have younger AFT dates than samples from similar elevations in the northern Ladakh batholith [*Kirstein et al*., 2009] across the Nubra strand of the KFZ (Figure 3 and 5). This continues the SW-NE trend of decreasing AFT dates across the Ladakh batholith, across the Nubra strand of the KFZ and into the Eastern Karakoram terrane. The results also permit differential uplift and erosional exhumation of the Eastern Karakoram relative to the Ladakh terrane due to a vertical component of motion on the Nubra strand. However, since the age groups overlap within uncertainty, localized vertical motion on the Nubra strand cannot be detected with confidence and is not required.

The AFT results from the Tangtse transect are within uncertainty of Nubra sample W11/41 from similar elevation (Figure 5). This suggests that the two subregions of the Eastern Karakoram terrane have followed a broadly similar low-temperature cooling history since at least approximately 5 Ma and that differential exhumation between them has been negligible since that time. This similarity in recent cooling histories is highlighted by the close similarity in modeled exhumation rates for the two regions (Table 3). Based on this similarity, the modeled exhumation rate data from the two regions can be combined to estimate an average exhumation rate of $0.67 + 0.27/-0.18$ mm/yr across the Eastern Karakoram terrane since approximately 7 Ma. For comparison, the apparent exhumation rate defined by the age-elevation relationship of the three Nubra samples lying on the main B-B′ transect is 0.51 mm/yr, with rates of 0.45–0.67 mm/yr being permissible within age uncertainty. Therefore, the two approaches give the same exhumation rates within uncertainty.

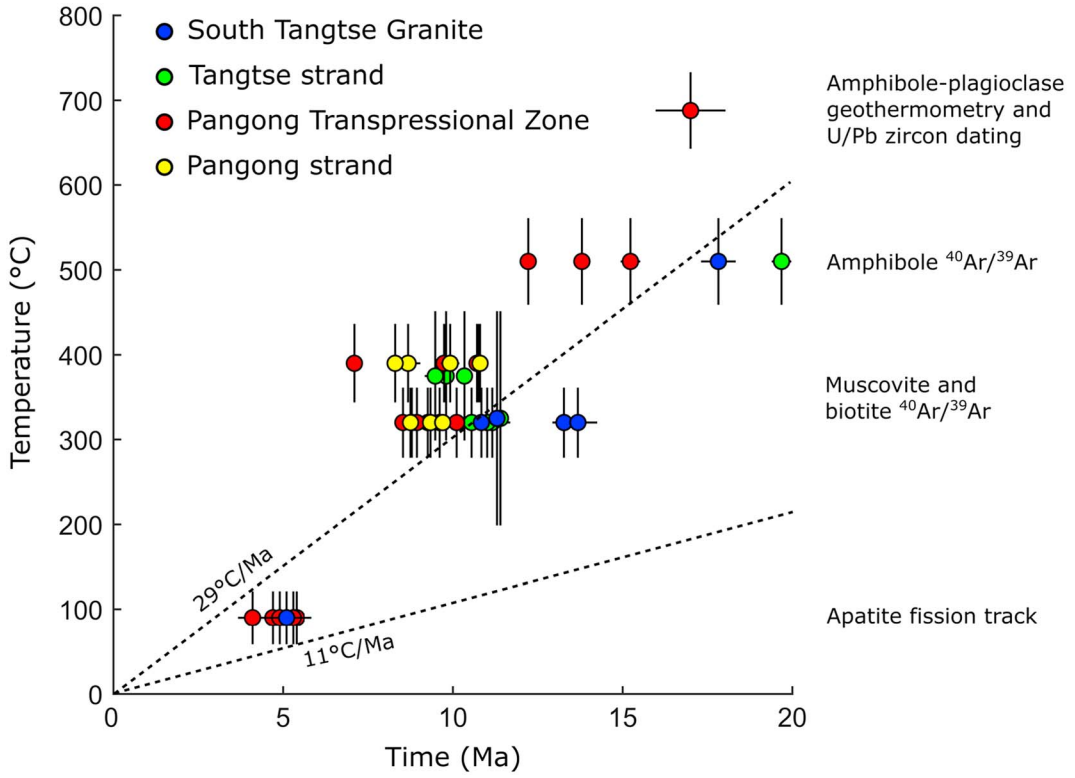

Figure 7. Compilation of temperature-time data from the Tangtse area, consisting of $^{40}Ar/^{39}Ar$ biotite, muscovite, and amphibole results [*Boutonnet et al*., 2012; *Dunlap et al*., 1998; *Mukherjee et al*., 2012; *Searle et al*., 1998] along with amphibole-plagioclase geothermometry [*Wallis et al*., 2014b] of the approximately 17 Ma migmatite unit [*Phillips et al*., 2013] and the fission track results of the present study. Data are divided into different portions of the Tangtse transect following *Boutonnet et al*. [2012]. An envelope of cooling rates is provided to aid interpretation, but note that these are not maximum and minimum permissible rates.

While few studies have investigated the temperature-time history of the Nubra area using geothermometry or thermochronology [*Bhutani et al*., 2003; *Wallis et al*., 2014b, 2015], the medium-high temperature cooling history of the Tangtse area is relatively well constrained [*Boutonnet et al*., 2012; *Dunlap et al*., 1998; *Mukherjee et al*., 2012; *Searle et al*., 1998; *Wallis et al*., 2014b]. The new AFT data reveal the low-temperature cooling history of the Tangtse area. Available temperature-time data for the Tangtse area are compiled in Figure 7. These consist primarily of $^{40}Ar/^{39}Ar$ biotite, muscovite, and amphibole results [*Boutonnet et al*., 2012; *Dunlap et al*., 1998; *Mukherjee et al*., 2012; *Searle et al*., 1998] along with amphibole-plagioclase geothermometry [*Wallis et al*., 2014b] of the approximately 17 Ma migmatite unit [*Phillips et al*., 2013] and the fission track results of the present study. We have not included high-temperature systems (e.g., zircon U/Pb) that record local and transient temperatures of emplacement of individual igneous intrusions, in order to focus on the longer-term cooling history of the wider country rocks.

It should be noted that the 41 data points represent a compilation from 32 samples across the approximately 8 km transect and that *Boutonnet et al*. [2012] recognized some variation in medium-temperature cooling histories between different portions of the transect. For instance, $^{40}Ar/^{39}Ar$ biotite and muscovite dates of approximately 7–11 Ma from the PTZ and Pangong strand (i.e., the NE portion of the transect) are somewhat younger than approximately 9–14 Ma dates from the Tangtse strand and South Tangtse granite (i.e., the SW portion of the transect). This contributes to the spread of $^{40}Ar/^{39}Ar$ biotite and muscovite dates evident in Figure 7. *Boutonnet et al*. [2012], who contributed the majority of the $^{40}Ar/^{39}Ar$ data, considered both plateau ages and inverse isochron ages to assess and minimize potential excess ^{40}Ar problems.

The new AFT data indicate cooling rates in the range 11–29°C/Ma between approximately 5 Ma and the present. However, the maximum cooling rate of 29°C/Ma is insufficient to explain the majority of the higher-temperature cooling ages. While the data from the south Tangtse granite can be explained by an

approximately constant cooling rate, all the other regions require higher cooling rates at some time interval (s) prior to cooling through the AFT partial annealing zone. In particular, the data from the PTZ require higher cooling rates between the approximately 5 Ma fission track ages and the approximately 7–11 Ma $^{40}Ar/^{39}Ar$ mica ages. These findings are broadly consistent with the interpretations of *Dunlap et al*. [1998] who suggested that transpressional fault motion since approximately 8 Ma caused an increase in uplift, exhumation, and cooling rates. The fission track results indicate that this phase of rapid cooling did not continue to the present day and that cooling rates reduced again some time since 7 Ma.

An important caveat to this analysis is that the geothermal gradient may not have remained constant over the timescales in question, in which case an increased cooling rate could occur at constant exhumation rate under a decreasing geothermal gradient. However, tectonic histories based on previous geothermobarometric and thermochronological studies of the region [e.g., *Kirstein*, 2011; *Wallis et al*., 2014b] provide no indication of, nor potential cause for, a temporary late Miocene to early Pliocene reduction in geothermal gradient.

In summary we find evidence that cooling of the PTZ was more rapid between the 7–8 Ma $^{40}Ar/^{39}Ar$ mica ages and the 5 Ma AFT ages than it was from 5 Ma to the present. The decrease in cooling rate suggests a switch to dominantly strike-slip fault motion along the PTZ and a concomitant reduction in its uplift relative to surrounding units. This is consistent with the geomorphology of the Pangong strand which has accommodated the majority of the recent deformation along the PTZ. Offset debris flows and alluvial fans along this strand indicate an average strike-slip slip rate of 4 ± 1 mm/yr since 14 ka and lack evidence for significant differential vertical motion on this strand [*Brown et al*., 2002]. Since this is the most geomorphologically prominent strand of the central KFZ, it is likely that the local surface expression of deformation continues to be dominantly strike slip at the present day.

5.1.1. Spatial Variation in Exhumation Rates Across Ladakh and the Karakoram

Low-temperature thermochronological data have delineated significant cooling age variations and trends across and between different portions of the western Himalaya-Karakoram. Extremely young AFT dates (<2 Ma) in the high Himalaya generally increase northward toward the Zanskar shear zone, a portion of the South Tibetan Detachment (approximately 15–19 Ma, Figure 1) [*Schulp et al*., 2011]. Farther NW, AFT dates decrease again across the Tso Morari dome (Figure 1) from approximately 30–40 Ma to approximately 7 Ma at the Indus suture [*Schulp et al*., 2003]. Across the Indus suture, a repeat of this trend is observed, with AFT dates decreasing systematically from 35–30 Ma to approximately 6 Ma across the Ladakh batholith [*Kirstein et al*., 2009]. Farther north in the central Karakoram, AFT dates are again very young, i.e., 2.1 ± 0.6 Ma to 4.3 ± 1.4 Ma (with one result of 31.5 ± 5.6 Ma) at extreme elevations of 5300 m to 8611 m on K2 [*Foster et al*., 1994]. This study fills an important gap in this transect across the Himalaya-Karakoram by providing AFT results from the Eastern Karakoram terrane, which is geographically and topographically intermediate between the Ladakh terrane and the central Karakoram.

The Eastern Karakoram terrane AFT dates, ranging between 3.3 ± 0.3 Ma and 7.4 ± 1.1 Ma (Table 2 and Figure 4), lie between the older ages from the Ladakh batholith to the SW and the younger ages from the central Karakoram to the NW, completing the trend across this region. This trend in cooling ages is reflected in a corresponding trend in modeled erosional exhumation rates which increase approximately sevenfold, from $0.09 + 0.03/-0.02$ mm/yr near the Indus suture to $0.67 + 0.27/-0.18$ mm/yr in the Eastern Karakoram terrane (Table 3 and Figure 6). As with the age data, the exhumation rate trend is continuous within uncertainty between the Ladakh terrane and the Eastern Karakoram terrane, suggesting that localized deformation along the Nubra strand of KFZ has had little or no impact on the erosional exhumation rates of the adjacent areas. A discontinuity in the exhumation rate trend appears to occur between the central and northern portions of the Ladakh terrane and may be associated with motion of the Khalsar thrust which separates these sample locations (Figure 3). However, targeted high spatial resolution sampling across the thrust trace would be required to test this hypothesis.

Kumar et al. [2007] analyzed AFT ages in more spatially restricted transects in the southern central portion of the Ladakh Range (including the younger ages near the bottom of Figure 3). They obtained exhumation rates of 0.09 and 0.11 mm/yr from age-elevation plots, in good agreement with our results. However, their shorter profiles do not record the long-range exhumation rate gradient across the Ladakh terrane and instead reflect more local erosional details (e.g., age-elevation relationships in individual valleys). It is possible that the younger ages on the southern slopes of the Ladakh terrane indicate some along-strike deviation from the exhumation rate trend in Figure 6, although more data along strike are required to test this hypothesis.

Foster et al. [1994] used AFT data from K2 to suggest exhumation rates of 3–6 mm/yr beginning at approximately 5–3 Ma followed by 0.5–1 mm/yr since approximately 2 Ma in this portion of the central Karakoram. These rates are similar to and somewhat higher than those from the Eastern Karakoram demonstrating that the trend of increasing exhumation rate continues north into the central Karakoram.

5.1.2. Causes of Regional Variation in Exhumation Rates

The combined data sets offer an opportunity to assess potential causes of the variation in exhumation rates across the different terranes. In particular, we consider the potential influences of climatic gradients and local and regional tectonic processes. The above synthesis of cooling age data and inferred exhumation rates demonstrates a long-range trend spanning the Ladakh and Karakoram terranes in which localized deformation associated with individual structures appears to have a relatively minor, second-order effect. For example, the KFZ strands have produced no discontinuity in the AFT age and exhumation rate trends that is clearly distinguishable from the longer-range trends. Similarly, the increase in exhumation rate across the Khalsar thrust, although more pronounced, is superimposed on the wider trend. Therefore, we suggest that the underlying driver of the exhumation rate trend acts over longer characteristic length scales of tens to hundreds of kilometers.

Present-day mean annual precipitation does vary over 100 km length scales across the region (Figure 2) [*Bookhagen and Burbank*, 2006, 2010; *Dortch et al*., 2013; *Palazzi et al*., 2013]. However, three considerations indicate that spatial variation in precipitation is not the cause of the exhumation rate trend. First, mean annual precipitation decreases from SW to NE, whereas exhumation rate increases (Figure 2). Second, unlike in the Himalaya to the south, precipitation varies little over the (tens of kilometers) length scales across which we observe strong exhumation rate gradients in our study area (Figure 2). Lastly, overall, precipitation is very low ($<$300 mm/yr) across eastern Ladakh and the Karakoram (Figure 2). Although these arguments are based on the present-day climate, it is unlikely that the direction of climatic gradients has typically been opposite (also with shorter wavelengths) over the past 7 Myrs.

Instead, we suggest that the trend in exhumation rates is a result of the long-wavelength gradient in crustal shortening and thickening from the Indus suture into the Karakoram. Crustal thickness increases from approximately 60 km beneath the Tethyan Himalaya to approximately 80 km beneath the central KFZ [*Hazarika et al*., 2014; *Rai et al*., 2006]. This thickening is associated with intense crustal shortening in the Karakoram, while the Ladakh batholith remains relatively undeformed [*Kirstein*, 2011; *Searle et al*., 2010]. In the central Karakoram, the surface expressions of this shortening and thickening are the extensive thrust systems, whereas major dome structures such as the Bullah and Dassu domes indicate more pervasive deformation at depth [*Searle et al*., 2010]. Although the Karakoram had a thickened Andean-type crust since the Cretaceous (M1, D1), geological relationships indicate multiple phases of postcollisional metamorphism and deformation (M2, D2 to M4, D4) [*Phillips et al*., 2013; *Searle et al*., 2010]. In particular, the M4-D4 Dassu dome contains sillimanite orthogneiss metamorphosed under conditions of 689 ± 48°C and 570 ± 190 MPa at 5.4 ± 0.1 Ma [*Fraser et al*., 2001; *Searle et al*., 2010]. This demonstrates crustal shortening and thickening associated with extremely rapid exhumation from approximately 20 km depth since the Pliocene, i.e., during the time span under consideration.

Since the India-Asia collision, rock uplift must have occurred at greater rates in the Karakoram than in surrounding regions such as the Ladakh terrane and Tibet. More material ($>$20 km) has been removed from parts of the Karakoram during the Neogene [*Fraser et al*., 2001; *Searle et al*., 2010; *Wallis et al*., 2014b] than from Ladakh since the Paleogene (7–14 km) [*Kirstein*, 2011]. Therefore, differential rock uplift must have occurred during the Neogene and/or Quaternary to avoid unfeasible paleotopography of the Karakoram originally having surface elevations 6–13 km higher than the Ladakh terrane.

As a result of their great elevation, the eastern and central Karakoram support extensive glacial systems throughout the glacial cycle, despite low levels of precipitation. In contrast, the lower elevations of the Ladakh terrane support less extensive glaciers and, for example, host only small cirque glaciers at the present day. We suggest that glacial erosion provides an effective mechanism for the removal of increasingly large amounts of material from south to north and results in the observed increase in exhumation rate. In other words, large-scale deformation, in the form of crustal shortening and thickening, provides the underlying driving force for rock and surface uplift, which ultimately results in glaciation despite the arid climate. Localized upper crustal deformation in fault zones is only the surface expression of this crustal shortening and thickening and appears to result in only second-order effects on patterns of exhumation. Although it is difficult to assess the roles of surface elevation and glaciation over million

year timescales, support for these interpretations is provided by studies of the late Pleistocene-Holocene glacial history and landscape evolution of the region [*Dortch et al*., 2010, 2011a, 2011b, 2013; *Munack et al*., 2014]. These provide a case study for how the system has behaved over the most recent glacial cycles and are summarized below.

5.2. Glaciation and Erosion in Ladakh and the Karakoram

Evidence for 19 glacial stages extending back to 311 ± 32 ka is preserved across the Ladakh-Karakoram region [*Dortch et al*., 2013], although older (now erased) glacial stages may have occurred earlier as the global climate cooled during the Pleistocene and late Neogene [*Raymo and Ruddiman*, 1992; *Zachos et al*., 2001]. Mapping of preserved glacial landforms has demonstrated that during the Deshkit 2 (81 ± 6 ka) and Deshkit 1 (45 ± 3 ka) glacial stages, glaciers in the Karakoram advanced such that the Siachen glacier extended approximately 100 km beyond its present limit, while those in the Ladakh Range extended only 9.2 ± 1.6 km and 2.7 ± 0.6 km respectively beyond their present limits [*Dortch et al*., 2010]. This suggests that although the absolute glacial cover may vary through time, the present-day trend of increasing glaciation from SW to NE is likely also typical of previous glacial cycles.

Support for the interpretation that tectonically generated high topography results in increased glacial cover and, in turn, increased erosion/exhumation rates is also provided by studies of the late Pleistocene history of glaciation and landscape evolution across the Ladakh-Karakoram regions. *Dortch et al*. [2011b] reached similar conclusions based on drainage morphometric analysis, mapping of present-day glaciers, and ^{10}Be dating of fluvial samples from the topographically asymmetrical Ladakh Range. They used the ^{10}Be inventories of fluvial sediments in active river channels draining catchments with varying extents of glaciation to determine catchment-wide erosion rates averaged over long (10^5 years) geomorphological timescales. They found that the topographically higher northern side of the range is associated with increased present-day glacial cover and higher erosion rates (between 0.056 ± 0.012 mm/yr and 0.074 ± 0.011 mm/yr since approximately 100 ka) than the southern side of the range (between 0.020 ± 0.003 mm/yr and 0.039 ± 0.008 mm/yr since approximately 300 ka).

Kirstein et al. [2009] and *Kirstein* [2011] suggested, based on AFT data, that the Ladakh batholith was tilted southward during the late Paleogene due to the ongoing collision, resulting in increased elevation and younger cooling ages in the north. Similarly, *Dortch et al*. [2011b] used published fluvial incision rates [*Dortch et al*., 2011a] to estimate a rock uplift rate of 0.6 mm/yr for the northern side of the Ladakh Range during the Quaternary. As this uplift is an order of magnitude faster than the erosion rate over similar timescales, they argued that denudational unloading was not a significant driver for tilting of the range. Rather, they concluded that ongoing tectonic uplift is raising the elevation of the northern side of the range, a process that could continue until sufficiently limited by the glacial equilibrium line altitude.

Munack et al. [2014] found that ^{10}Be data from the Indus valley, along the southern margin of the Ladakh Range, spanning postglacial timescales of 10^3–10^4 years, indicate denudation rates of only 0.01–0.11 mm yr^{-1}. As these rates are lower than those derived from low-temperature thermochronological data spanning greater timescales of $>10^6$ years (approximately 0.1–0.4 mm yr^{-1}) [*Clift et al*., 2002; *Kirstein et al*., 2006, 2009; *Kirstein*, 2011; *Kumar et al*., 2007; *Sinclair and Jaffey*, 2001, this study], the authors concluded that glacial processes during previous glacial cycles must have made a significant contribution to erosional denudation and rock exhumation and cooling.

Our findings are comparable to several recent studies documenting the tectonic processes of the India-Asia collision as the underlying driving forces for mountain range growth and rock exhumation along much of the Himalaya [e.g., *Adams et al*., 2015; *Burbank et al*., 2003; *Godard et al*., 2014; *Robert et al*., 2011; *Thiede and Ehlers*, 2013; *Wang et al*., 2014]. For instance, the recent review of *Thiede and Ehlers* [2013], based on thermal-kinematic erosion modeling of 1126 Himalayan bedrock cooling ages, emphasized the importance of both tectonic deformation and glacial processes in controlling spatial and temporal variations in erosional denudation. We find that these processes are also key controls on mountain range evolution behind the Himalayan front in Ladakh and the Karakoram where climatic influences such as the monsoon are suppressed [*Bookhagen and Burbank*, 2010; *Palazzi et al*., 2013] and the impacts of tectonic deformation and rock uplift are highlighted.

6. Conclusions

Apatite fission track analysis of 10 samples from two transects across the central KFZ in the Eastern Karakoram range gives cooling ages between 3.3 ± 0.3 Ma and 7.4 ± 1.1 Ma, providing the first constraints on the

low-temperature cooling history of the Eastern Karakoram terrane. The data allow modeling of erosional exhumation rates which average 0.67 + 0.27/−0.18 mm/yr across the Eastern Karakoram terrane since approximately 7.4 Ma. The new results elucidate significant variations in AFT ages and exhumation rates between different tectonic domains across Ladakh and the Karakoram. In particular, the Eastern Karakoram results show that the trend of increasing exhumation rate across the Ladakh batholith (from 0.09 + 0.03/−0.02 mm/yr to 0.47 + 0.44/−0.18 mm/yr), apparent in the data of *Kirstein et al*. [2009], continues northeast into the Karakoram terrane. Farther to the northwest within the central Karakoram terrane, cooling ages are younger still [*Foster et al*., 1994]. Overall, the results complete a south-north trend of increasing exhumation rate from the Indus suture, across the Ladakh batholith and into the Karakoram.

Across the region where we have detected the trend in exhumation rates there is little variation in present-day mean annual precipitation and, at the broader scale, precipitation decreases SW-NE, making spatial variation in climate an unlikely cause of the exhumation rate trends. However, the extent of glaciation increases SW-NE across the study area and geomorphological evidence suggest that this has been the case since at least the late Pleistocene [*Dortch et al*., 2010]. Therefore, we advocate a model in which spatial variations in exhumation rates in this portion of the orogen are primarily driven by spatial variations in the vertical component of rock motion. This in turn is driven by regional tectonics of crustal thickening. The associated surface uplift promotes glaciation and generation of extreme relief, even where mean precipitation is relatively low, facilitating high erosion rates which contribute to rapid exhumation.

Acknowledgments
The data reported in this paper are also available on request from the corresponding author. D.W. acknowledges support from NERC (training grant NE/I528750/1). Hannah Watkins and Fida Hussain Mitoo are thanked for their assistance during fieldwork. We thank Lindsay Schoenbohm, Pierre Valla, and an anonymous reviewer for their constructive comments which helped to improve the paper.

References

Adams, B. A., K. V. Hodges, K. X. Whipple, T. A. Ehlers, M. C. van Soest, and J. Wartho (2015), Constraints on the tectonic and landscape evolution of the/Bhutan Himalaya from thermochronometry, *Tectonics*, *34*, 1329–1347, doi:10.1002/2015TC003853.

Banerjee, P., and R. Bürgmann (2002), Convergence across the northwest Himalaya from GPS measurements, *Geophys. Res. Lett.*, *29*(13, 1652), doi:10.1029/2002GL015184.

Beaumont, C., R. A. Jamieson, M. H. Nguyen, and B. Lee (2001), Himalayan tectonics explained by extrusion of a low-viscosity crustal channel coupled to focused surface denudation, *Nature*, *414*, 738–742, doi:10.1038/414738a.

Bhutani, R., K. Pande, and N. Desai (2003), Age of the Karakoram fault activation: ^{40}Ar-^{39}Ar geochronological study of Shyok suture zone in northern Ladakh, India, *Curr. Sci.*, *84*, 1454–1458, doi:10.1016/j.jseaes.2008.03.013.

Bhutiyani, M. R., V. S. Kale, and N. J. Pawar (2007), Long-term trends in maximum, minimum and mean annual air temperatures across the Northwestern Himalaya during the twentieth century, *Clim. Change*, *85*, 159–177, doi:10.1007/s10584-006-9196-1.

Bishop, M. P., A. B. G. Bush, L. Copland, K. Ulrich, L. A. Owen, Y. B. Seong, and J. F. Schroder Jr. (2010), Climate change and mountain topographic evolution in the central Karakoram, Pakistan, *Ann. Assoc. Am. Geogr.*, *100*, 772–793, doi:10.1080/00045608.2010.500521.

Bookhagen, B., and D. W. Burbank (2006), Topography, relief, and TRMM-derived rainfall variations along the Himalaya, *Geophys. Res. Lett.*, *33*, L08405, doi:10.1029/2006GL026037.

Bookhagen, B., and D. W. Burbank (2010), Toward a complete Himalayan hydrological budget: Spatiotemporal distribution of snowmelt and rainfall and their impact on river discharge, *J. Geophys. Res.*, *115*, F03019, doi:10.1029/2009JF001426.

Boutonnet, E., P. H. Leloup, N. Arnaud, J.-L. Paquette, W. J. Davis, and K. Hattori (2012), Synkinematic magmatism, heterogeneous deformation, and progressive strain localization in a strike-slip shear zone: The case of the right-lateral Karakorum fault, *Tectonics*, *31*, TC4012, doi:10.1029/2011TC003049.

Brown, E. T., R. Bendick, D. L. Bourlès, V. Gaur, P. Molnar, G. M. Raisbeck, and F. Yiou (2002), Slip rates of the Karakorum fault, Ladakh, India, determined using cosmic ray exposure dating of debris flows and moraines, *J. Geophys. Res.*, *107*(B9), 2192, doi:10.1029/2000JB000100.

Brozović, N., D. W. Burbank, and A. J. Meigs (1997), Climatic limits on landscape development in the northwestern Himalaya, *Science*, *276*, 571–574, doi:10.1126/science.276.5312.571.

Burbank, D. W., A. E. Blythe, J. Putkonen, B. Pratt-Sitaula, E. Gabet, M. Oskin, A. Barros, and T. P. Ojha (2003), Decoupling of erosion and precipitation in the Himalayas, *Nature*, *426*, 652–655, doi:10.1038/nature02187.

Cerveny, P. F., C. W. Naeser, P. B. Keleman, J. E. Lieberman, and P. K. Zeitler (1989), Zircon fission-track ages from the Gasherbrum Diorite, Karakoram Range, northern Pakistan, *Geology*, *17*, 1044–1048, doi:10.1130/0091-7613(1989)017<1044:ZFTAFT>2.3.CO;2.

Chevalier, M.-L., P. Tapponnier, J. Van der Woerd, F. J. Ryerson, R. C. Finkel, and H. Li (2012), Spatially constant slip rate along the southern segment of the Karakorum fault since 200 ka, *Tectonophysics*, *530*, 152–179, doi:10.1016/j.tecto.2011.12.014.

Choubey, V. M. (1987), Fission track geochronology of the southern part of the Ladakh batholith, Ladakh, northwest Himalaya, *Geosci. J.*, *8*, 73–80.

Clift, P. D., A. Carter, M. Krol, and E. Kirby (2002), Constraints on India-Eurasia collision in the Arabian Sea region taken from the Indus Group, Ladakh Himalaya, India, in *The Tectonic and Climatic Evolution of the Arabian Sea Region*, *Geol. Soc. London, Spec. Publ.*, vol. 195, edited by P. D. Clift et al., pp. 97–116, Geological Society, London, doi:10.1144/GSL.SP.2002.195.01.07.

Dortch, J. M., L. A. Owen, and M. W. Caffee (2010), Quaternary glaciation in the Nubra and Shyok valley confluence, northernmost Ladakh, India, *Quat. Res.*, *74*, 132–144, doi:10.1016/j.yqres.2010.04.013.

Dortch, J. M., C. Dietsch, L. A. Owen, M. W. Caffee, and K. Ruppert (2011a), Episodic fluvial incision of rivers and rock uplift in the Himalaya and Transhimalaya, *J. Geol. Soc. Lond.*, *168*, 783–804, doi:10.1144/0016-76492009-158.

Dortch, J. M., L. A. Owen, L. M. Schoenbohm, and M. W. Caffee (2011b), Asymmetrical erosion and morphological development of the central Ladakh Range, northern India, *Geomorphology*, *135*, 167–180, doi:10.1016/j.geomorph.2011.08.014.

Dortch, J. M., L. A. Owen, and M. W. Caffee (2013), Timing and climatic drivers for glaciation across semi-arid western Himalayan-Tibetan orogen, *Quat. Sci. Rev.*, *78*, 188–208, doi:10.1016/j.quascirev.2013.07.025.

Dunlap, W. J., R. F. Weinberg, and M. P. Searle (1998), Karakoram fault zone rocks cool in two phases, *J. Geol. Soc.*, *155*, 903–912, doi:10.1144/gsjgs.155.6.0903.

Egholm, D. L., S. B. Nielsen, V. K. Pedersen, and J.-E. Lesemann (2009), Glacial effects limiting mountain height, *Nature*, *460*, 884–887, doi:10.1038/nature08263.
Foster, D. A., A. J. W. Gleadow, and G. Mortimer (1994), Rapid Pliocene exhumation in the Karakoram (Pakistan), revealed by fission-track thermochronology of the K2 gneiss, *Geology*, *22*, 19–22, doi:10.1130/0091-7613(1994)022<0019:RPEITK>2.3.CO;2.
Fraser, J. E., M. P. Searle, R. R. Parrish, and S. R. Nobel (2001), Chronology of deformation, metamorphism, and magmatism in the southern Karakoram Mountains, *Geol. Soc. Am. Bull.*, *113*, 1443–1455, doi:10.1130/0016-7606.
Godard, V., D. L. Bourles, F. Spinabella, D. W. Burbank, B. Bookhagen, G. B. Fisher, A. Moulin, and L. Leanni (2014), Dominance of tectonics over climate in Himalayan denudation, *Geology*, *42*, 243–246, doi:10.1130/G35342.1.
Hazarika, D., K. Sen, and N. Kumar (2014), Characterizing the intracrustal low velocity zone beneath northwest India-Asia collision zone, *Geophys. J. Int.*, *199*, 1338–1353, doi:10.1093/gji/ggu328.
Hobley, D. E. J., H. D. Sinclair, and S. M. Mudd (2012), Reconstruction of a major storm even from its geomorphic signature: The Ladakh floods, 6 August 2010, *Geology*, *40*, 483–486, doi:10.1130/G32935.1.
Hurford, A. J. (1990), Standardization of fission track dating calibration: Recommendation by the Fission Track Working Group of the IUGS subcommission on geochronology, *Chem. Geol.*, *80*, 177–178, doi:10.1016/0168-9622(90)90025-8.
Jade, S., B. C. Bhatt, Z. Yang, R. Bendick, V. K. Gaur, P. Molnar, M. B. Anand, and D. Kumar (2004), GPS measurements from the Ladakh Himalaya, India: Preliminary tests of plate-like or continuous deformation in Tibet, *Geol. Soc. Am. Bull.*, *116*, 1385–1391, doi:10.1130/B25357.1.
Jade, S., H. J. Raghavendra Rao, M. S. M. Vijayan, V. K. Gaur, B. C. Bhatt, K. Kumar, S. Jaganathan, M. B. Ananda, and P. Dileep Kumar (2010), GPS-derived deformation rates in northwestern Himalaya and Ladakh, *Int. J. Earth Sci.*, *100*, 1293–1301, doi:10.1007/s00531-010-0532-3.
Kirstein, L., H. Sinclair, F. M. Stuart, and K. Dobson (2006), Rapid early Miocene exhumation of the Ladakh batholith, western Himalaya, *Geology*, *34*, 1049–1052, doi:10.1130/G22857A.1.
Kirstein, L. A. (2011), Thermal evolution and exhumation of the Ladakh Batholith, northwest Himalaya, India, *Tectonophysics*, *503*, 222–233, doi:10.1016/j.tecto.2011.03.005.
Kirstein, L. A., J. P. T. Foeken, P. van der Beek, F. M. Stuart, and R. J. Phillips (2009), Cenozoic unroofing history of the Ladakh Batholith, western Himalaya, constrained by thermochronology and numerical modelling, *J. Geol. Soc.*, *166*, 667–678, doi:10.1144/0016-76492008-107.
Korinkova, D., M. Svojtka, and J. Kalvoda (2014), Rate of erosion and exhumation of crystalline rocks in the Hunza Karakoram defined by apatite fission track analysis, *Acta Geodyn. Geomater.*, *11*, 235–253, doi:10.13168/AGG.2014.0010.
Kumar, R., N. Lai, S. Singh, and A. K. Jain (2007), Cooling and exhumation of the Transhimalayan Ladakh batholith as constrained by fission track apatite and zircon ages, *Curr. Sci.*, *92*, 490–496.
Lacassin, R., et al. (2004), Large-scale geometry, offset and kinematic evolution of the Karakorum fault, Tibet, *Earth Planet. Sci. Lett.*, *219*, 255–269, doi:10.1016/S0012-821X(04)00006-8.
Lavé, J., and J. P. Avouac (2001), Fluvial incision and tectonic uplift across the Himalayas of central Nepal, *J. Geophys. Res.*, *106*, 26,561–26,591, doi:10.1029/2001JB000359.
Leloup, P. H., E. Boutonnet, J. D. William, and K. Hattori (2011), Long-lasting intracontinental strike-slip faulting: New evidence from the Karakorum shear zone in the Himalayas, *Terra Nova*, *23*, 92–99, doi:10.1111/j.1365-3121.2011.00988.x.
Molnar, P., P. England, and J. Martinod (1993), Mantle dynamics, uplift of the Tibetan Plateau, and the Indian monsoon, *Rev. Geophys.*, *31*, 357–396, doi:10.1029/93RG02030.
Mukherjee, B. K., K. Sen, H. K. Sachan, and S. K. Paul (2012), Exhumation history of the Karakoram fault zone mylonites: New constraints from microstructures, fluid inclusions and ^{40}Ar-^{39}Ar analyses, *Lithosphere*, *4*, 230–241, doi:10.1130/L163.1.
Munack, H., O. Korup, A. Resentini, M. Limonta, E. Garzanti, J. H. Blöthe, D. Scherler, H. Wittmann, and P. W. Kubik (2014), Postglacial denudation of western Tibetan Plateau margin outpaced by long-term exhumation, *Geol. Soc. Am. Bull.*, *126*, 1580–1594, doi:10.1130/B30979.1.
Najman, Y., et al. (2010), Timing of India-Asia collision: Geological, biostratigraphic, and palaeomagnetic constraints, *J. Geophys. Res.*, *115*, B12416, doi:10.1029/2010JB007673.
Palazzi, E., J. von Hardenberg, and A. Provenzale (2013), Precipitation in the Hindu-Kush Karakoram Himalaya: Observations and future scenarios, *J. Geophys. Res. Atmos.*, *118*, 85–100, doi:10.1029/2012JD018697.
Phartiyal, B., and A. Sharma (2009), Soft-sediment deformation structures in the Late Quaternary sediments of Ladakh: Evidence for multiple phases of seismic tremors in the North western Himalayan Region, *J. Asian Earth Sci.*, *34*, 761–770, doi:10.1016/j.jseaes.2008.11.008.
Phartiyal, B., A. Sharma, R. Upadhyaya, R. Awatar, and A. K. Sinha (2005), Quaternary geology, tectonics and distribution of palaeo- and present fluvio/glacio lacustrine deposits in Ladakh, NW Indian Himalaya—A study based on field observations, *Geomorphology*, *65*, 214–256, doi:10.1016/j.geomorph.2004.09.004.
Phillips, R. J. (2008), Geological map of the Karakoram Fault zone, Eastern Karakoram, Ladakh, NW Himalaya, *J. Maps*, *2008*, 38–49, doi:10.4113/jom.2008.93.
Phillips, R. J., and M. P. Searle (2007), Macrostructural and microstructural architecture of the Karakoram fault: Relationship between magmatism and strike-slip faulting, *Tectonics*, *26*, TC3017, doi:10.1029/2006TC001946.
Phillips, R. J., R. R. Parrish, and M. P. Searle (2004), Age constraints on ductile deformation and long-term slip rates along the Karakoram fault zone, Ladakh, *Earth Planet. Sci. Lett.*, *226*, 305–319, doi:10.1016/j.epsl.2004.07.037.
Phillips, R. J., M. P. Searle, and R. R. Parrish (2013), The geochemical and temporal evolution of the continental lithosphere and its relationship to continental-scale faulting: The Karakoram Fault, Eastern Karakoram, NW Himalayas, *Geochem. Geophys. Geosyst.*, *14*, 583–603, doi:10.1002/ggge.20061.
Rai, S. S., K. Priestly, V. K. Guar, S. Mitra, M. P. Singh, and M. P. Searle (2006), Configuration of the Indian Moho beneath the NW Himalaya and Ladakh, *Geophys. Res. Lett.*, *33*, L15308, doi:10.1029/2006GL026076.
Raymo, M. E., and W. F. Ruddiman (1992), Tectonic forcing of late Cenozoic climate, *Nature*, *359*, 117–122.
Reichardt, H., and R. F. Weinberg (2012), Hornblende chemistry in meta- and diatexites and its retention in the source of leucogranites: An example from the Karakoram Shear Zone, NW India, *J. Petrol.*, *53*, 1287–1318, doi:10.1093/petrology/egs017.
Reichardt, H., R. F. Weinberg, U. B. Andersson, and C. M. Fanning (2010), Hybridization of granitic magmas in the source: The origin of the Karakoram Batholith, Ladakh, NW India, *Lithos*, *116*, 249–272, doi:10.1016/j.lithos.2009.11.013.
Reiners, P. W., and M. T. Brandon (2006), Using thermochronology to understand orogenic erosion, *Annu. Rev. Earth Planet. Sci.*, *34*, 419–66, doi:10.1146/annurev.earth.34.031405.125202.
Robert, X., P. van der Beek, J. Braun, C. Perry, and J.-L. Mugnier (2011), Control of detachment geometry on lateral variations in exhumation rates in the Himalaya: Insights from low-temperature thermochronology and numerical modelling, *J. Geophys. Res.*, *116*, B05202, doi:10.1029/2010JB007893.
Robinson, A. C. (2009), Evidence against Quaternary slip on the northern Karakorum Fault suggests kinematic reorganisation at the western end of the Himalayan-Tibetan orogen, *Earth Planet. Sci. Lett.*, *286*, 158–170, doi:10.1016/j.epsl.2009.06.025.

Rutter, E. H., D. R. Faulkner, K. H. Brodie, R. J. Phillips, and M. P. Searle (2007), Rock deformation processes in the Karakoram fault zone, Ladakh, NW India, *J. Struct. Geol.*, *29*, 1315–1326, doi:10.1016/j.jsg.2007.05.001.

Ryan, W. B. F., et al. (2009), Global multi-resolution topography synthesis, *Geochem. Geophys. Geosyst.*, *10*, Q03014, doi:10.1029/2008GC002332.

Schulp, M., A. Carter, M. Cosca, and A. Steck (2003), Exhumation history of eastern Ladakh revealed by ^{40}Ar-^{39}Ar and fission track ages: The Indus River-Tso Morari transect, NW Himalaya, *J. Geol. Soc.*, *160*, 385–399, doi:10.1144/0016-764902-084.

Schulp, M., A. Steck, A. Carter, M. Cosca, J.-L. Epard, and J. Hunziker (2011), Exhumation history of the NW Indian Himalaya revealed by fission track and ^{40}Ar/^{39}Ar ages, *J. Asian Earth Sci.*, *40*, 334–350, doi:10.1016/j.jseaes.2010.06.008.

Searle, M. P. (1991), *Geology and Tectonics of the Karakoram Mountains*, pp. 376, John Wiley, Chichester.

Searle, M. P. (1996), Geological evidence against large-scale pre-Holocene offsets along the Karakoram Fault: Implications for the limited extrusion of the Tibetan Plateau, *Tectonics*, *15*, 171–186, doi:10.1029/95TC01693.

Searle, M. P., and R. J. Phillips (2007), Relationships between right-lateral shear along the Karakoram fault and metamorphism, magmatism, exhumation and uplift: Evidence from the K2-Gasherbrum-Pangong ranges, north Pakistan and Ladakh, *J. Geol. Soc.*, *164*, 439–450, doi:10.1144/0016-76492006-072.

Searle, M. P., R. R. Parrish, R. Tirrul, and D. C. Rex (1990), Age of crystallisation and cooling of the K2 gneiss and the Baltoro Karakoram, *J. Geol. Soc. Lond.*, *147*, 603–606, doi:10.1144/gsjgs.147.4.0603.

Searle, M. P., R. F. Weinberg, and W. J. Dunlap (1998), Transpressional tectonics along the Karakoram fault zone, northern Ladakh: Constraints on Tibetan extrusion, in *Continental Transpressional and Transtensional Tectonics*, edited by R. E. Holdsworth et al., *Geol. Soc. London, Spec. Publ.*, *135*, 307–326, doi:10.1144/GSL.SP.1998.135.01.20.

Searle, M. P., R. R. Parrish, A. V. Thow, S. R. Noble, R. J. Phillips, and D. J. Waters (2010), Anatomy, age and evolution of a collisional mountain belt: The Baltoro batholith and Karakoram Metamorphic Complex, Pakistani Karakoram, *J. Geol. Soc.*, *167*, 183–202, doi:10.1144/0016-76492009-043.

Searle, M. P., J. R. Elliott, R. J. Phillips, and S.-L. Chung (2011), Crustal-lithospheric structure and continental extrusion of Tibet, *J. Geol. Soc.*, *168*, 633–672, doi:10.1144/0016-76492010-139.

Sen, K., B. K. Mukherjee, and A. S. Collins (2014), Interplay of deformation and magmatism in the Pangong Transpressional Zone, Eastern Ladakh, India: Implications for remobilization of the trans-Himalayan magmatic arc and initiation of the Karakoram Fault, *J. Struct. Geol.*, *62*, 13–24, doi:10.1016/j.jsg.2014.01.009.

Sinclair, H. D., and N. Jaffey (2001), Sedimentology of the Indus Group, Ladakh, northern India: Implications for the timing of initiation of the palaeo-Indus River, *J. Geol. Soc.*, *158*, 151–162, doi:10.1144/jgs.158.1.151.

Sinha, A. K., H. Rai, R. Uphadhyay, and R. Chandra (1999), Contribution to the geology of the Eastern Karakoram, India, in *Himalaya and Tibet: Mountain Roots to Mountain Tops*, vol. 328, edited by A. Macfarlane, R. B. Sorkhabi, and J. Quade, pp. 33–46, Geol. Soc. Am. Spec. Pap., Boulder, Colo.

Sorkhabi, R. B., A. K. Jain, S. Nishimura, T. Itaya, N. Lai, R. M. Manickavasagam, and T. Tagami (1994), New age constraints on the cooling and unroofing history of the Trans-Himalayan Ladakh Batholith (Kargil area), N.W. India, *Proc. Indian Acad. Sci.*, *103*, 83–97, doi:10.1007/BF02880810.

St-Onge, M. R., N. Rayner, and M. P. Searle (2010), Zircon age determinations for the Ladakh batholith at Chumatang (Northwest India): Implications for the age of the India-Asia collision in the Ladakh Himalaya, *Tectonophysics*, *495*, 171–183, doi:10.1016/j.tecto.2010.09.010.

Streule, M. J., R. J. Phillips, M. P. Searle, D. J. Waters, and M. S. A. Horstwood (2009), Evolution and chronology of the Pangong Metamorphic Complex adjacent to the Karakoram Fault, Ladakh: Constraints from thermobarometry metamorphic modelling and U-Pb geochronology, *J. Geol. Soc.*, *166*, 919–932, doi:10.1144/0016-76492008-117.

Thiede, R. C., and T. A. Ehlers (2013), Large spatial and temporal variations in Himalayan denudation, *Earth Planet. Sci. Lett.*, *371*, 278–293, doi:10.1016/j.epsl.2013.03.004.

Thiede, R. C., B. Bookhagen, J. R. Arrowsmith, E. R. Sobel, and M. R. Strecker (2004), Climatic control on rapid exhumation along the Southern Himalayan Front, *Earth Planet. Sci. Lett.*, *222*, 791–806, doi:10.1016/j.epsl.2004.03.015.

Thomson, S. N., M. T. Brandon, J. H. Tomkin, P. W. Reiners, C. Vásquez, and N. J. Wilson (2010), Glaciation as a destructive and constructive control on mountain building, *Nature*, *467*, 313–317, doi:10.1038/nature09365.

Upadhyay, R. (2001), Seismically-induced soft-sediment deformational structures around Khalsar in the Shyok Valley, northern Ladakh and Eastern Karakoram, India, *Curr. Sci.*, *81*, 600–604.

Upadhyay, R. (2003), Earthquake-induced soft-sediment deformation in the lower Shyok river valley, northern Ladakh, India, *J. Asian Earth Sci.*, *21*, 413–421, doi:10.1016/S1367-9120(02)00033-0.

Wallis, D., R. J. Phillips, and G. E. Lloyd (2013), Fault weakening across the frictional-viscous transition zone, Karakoram Fault Zone, NW Himalaya, *Tectonics*, *32*, 1227–1246, doi:10.1002/tect.20076.

Wallis, D., A. J. Parsons, R. J. Phillips, M. P. Searle, and E. C. Ferré (2014a), Comment on "Interplay of deformation and magmatism in the Pangong Transpressional Zone, eastern Ladakh, India: Implications for remobilization of the trans-Himalayan magmatic arc and initiation of the Karakoram Fault" by K. Sen, B.K. Mukherjee and A.S. Collins, Journal of Structural Geology 62 (2014) 13-24, *J. Struct. Geol.*, *65*, 117–119, doi:10.1016/j.jsg.2014.03.008.

Wallis, D., R. J. Phillips, and G. E. Lloyd (2014b), Evolution of the Eastern Karakoram Metamorphic Complex, Ladakh, NW India, and its relationship to magmatism and regional tectonics, *Tectonophysics*, *626*, 41–52, doi:10.1016/j.tecto.2014.03.023.

Wallis, D., G. E. Lloyd, R. J. Phillips, A. J. Parsons, and R. D. Walshaw (2015), Low effective fault strength due to frictional-viscous flow in phyllonites, Karakoram Fault Zone, NW India, *J. Struct. Geol.*, *77*, 45–61, doi:10.1016/j.jsg.2015.05.010.

Wang, H., and T. J. Wright (2012), Satellite geodetic imaging reveals internal deformation of western Tibet, *Geophys. Res. Lett.*, *39*, L07303, doi:10.1029/2012GL051222.

Wang, P., D. Scherler, J. Liu-Zeng, J. Mey, J.-P. Avouac, Y. Zhang, and D. Shi (2014), Tectonic control of Yarlung Tsangpo Gorge revealed by a buried canyon in Southern Tibet, *Science*, *346*, 978–981, doi:10.1126/science.1259041.

Wang, S., C. Wang, R. J. Phillips, M. A. Murphy, X. Fang, and Y. Yue (2012), Displacement along the Karakoram fault, NW Himalaya, estimated from LA-ICP-MS U-Pb dating of offset geologic markers, *Earth Planet. Sci. Lett.*, *337*, 156–163, doi:10.1016/j.epsl.2012.05.037.

Wang, S., Y. Mo, R. J. Phillips, and C. Wang (2013), Karakoram fault activity defined by temporal constraints on the Ayi Shan detachment, SW Tibet, *Int. Geol. Rev.*, *56*, 15–28, doi:10.1080/00206814.2013.818750.

Weinberg, R. F., W. J. Dunlap, and M. Whitehouse (2000), New field, structural and geochronological data from the Shyok and Nubra valleys, northern Ladakh: Linking Kohistan to Tibet, in *Tectonics of the Nanga Parbat Syntaxis and the Western Himalaya*, edited by M. A. Khan et al., *Geol. Soc. London, Spec. Publ.*, *170*, 253–275, doi:10.1144/GSL.SP.2000.170.01.14.

Willett, S. D., and M. T. Brandon (2013), Some analytical methods for converting thermochronometric age to erosion rate, *Geochem. Geophys. Geosyst.*, *14*, 209–222, doi:10.1029/2012GC004279.

Wittlinger, G., J. Vergne, P. Tapponnier, V. Farra, G. Poupinet, M. Jiang, H. Su, G. Herquel, and A. Paul (2004), Teleseismic imaging of subducting lithosphere and Moho offsets beneath western Tibet, *Earth Planet. Sci. Lett.*, *221*, 117–130, doi:10.1016/S0012-821X(03)00723-4.

Zachos, J., M. Pagini, L. Sloan, E. Thomas, and K. Billups (2001), Trends, rhythms, and aberrations in global climate 65 Ma to present, *Science*, *292*, 686–693.

Zeitler, P. K., et al. (2001), Erosion, Himalayan geodynamics, and the geomorphology of metamorphism, *GSA Today*, *11*, 4–9, doi:10.1130/1052-5173(2001)011<0004:EHGATG>2.0.CO;2.

Zhang, R., M. A. Murphy, T. Lapen, V. Sanchez, and M. Heizler (2011), Late Eocene crustal thickening followed by Early-Late Oligocene extension along the India-Asia suture zone: Evidence for cyclicity in the Himalayan orogen, *Geosphere*, *7*, 1249–1268, doi:10.1130/GES00643.1.